Evaluation of the osteoinductive potential of a bio-inspired scaffold mimicking the osteogenic niche for bone augmentation

Silvia Minardi [a, b], Bruna Corradetti [b, c], Francesca Taraballi [b], Monica Sandri [a], Jeffrey Van Eps [b, d], Fernando J. Cabrera [b], Bradley K. Weiner [b, e], Anna Tampieri [a], Ennio Tasciotti [b, *]

[a] Institute of Science and Technology for Ceramics — CNR, Via Granarolo 64, 48018, Faenza, RA, Italy
[b] Department of Nanomedicine, Houston Methodist Research Institute, 6670 Bertner Ave., Houston, TX, 77030, USA
[c] Department of Life and Environmental Sciences, Universita' Politecnica delle Marche, Via Brecce Bianche, 60131, Ancona, Italy
[d] Department of Surgery, Houston Methodist Hospital, 6550 Fannin St., Houston, TX, 77030, USA
[e] Department of Orthopedics & Sports Medicine, Houston Methodist Hospital, 6550 Fannin St., Houston, TX, 77030, USA

ARTICLE INFO

ABSTRACT

Augmentation of regenerative osteogenesis represents a premier clinical need, as hundreds of thousands of patients are left with insufficient healing of bony defects related to a host of insults ranging from congenital abnormalities to traumatic injury to surgically-induced deficits. A synthetic material that closely mimics the composition and structure of the human osteogenic niche represents great potential to successfully address this high demand. In this study, a magnesium-doped hydroxyapatite/type I collagen scaffold was fabricated through a biologically-inspired mineralization process and designed to mimic human trabecular bone. The composition of the scaffold was fully characterized by XRD, FTIR, ICP and TGA, and compared to human bone. Also, the scaffold microstructure was evaluated by SEM, while its nano-structure and nano-mechanical properties were evaluated by AFM. Human bone marrow-derived mesenchymal stem cells were used to test the in vitro capability of the scaffold to promote osteogenic differentiation. The cell/scaffold constructs were cultured up to 7 days and the adhesion, organization and proliferation of the cells were evaluated. The ability of the scaffold to induce osteogenic differentiation of the cells was assessed over 3 weeks and the correlate gene expression for classic genes of osteogenesis was assessed. Finally, when tested in an ectopic model in rabbit, the scaffold produced a large volume of trabecular bone in only two weeks, that subsequently underwent maturation over time as expected, with increased mature cortical bone formation, supporting its ability to promote bone regeneration in clinically-relevant scenarios. Altogether, these results confirm a high level of structural mimicry by the scaffold to the composition and structure of human osteogenic niche that translated to faster and more efficient osteoinduction in vivo — features that suggest such a biomaterial may have great utility in future clinical applications where bone regeneration is required.

1. Introduction

Bone augmentation is defined as the increase in osseous dimensions achieved via the addition of material or tissue [1]. It has become common clinical practice in a variety of medical conditions in which functional restoration of damaged bone is needed - such as traumatic injury, degenerative diseases, congenital deformities, cancer, or in post-operative defects [2,3]. Autologous trabecular bone is widely regarded as the standard for bone augmentation, supplying growth factors, cells and a mechanical support for tissue's structure [4,5]. The iliac crest is currently the principal source of autologous bone for such applications, however, donor site morbidity, higher care cost from longer hospital stays or surgical complication, and additional subsequent surgery are just some of several limitations of this approach [4,6]. Allografts have been investigated as an alternative strategy, but immunogenic rejection and risk for disease transmission have never been fully resolved [7]. These limitations have spurred the development of a plethora of

synthetic grafting materials in recent decades [8]. The main advantages of off-the-shelf materials include: lower cost, biocompatibility, biosafety, lower risk of rejection and simplification of the procedure to a single operation [9]. First generation synthetic materials were lacking in osteoinductive and osteogenic elements and their rate of success was inferior to autologous or allogenic bone grafts [10]. More recent decades have witnessed great progress in understanding the key osteogenic cues that synthetic materials must provide for efficient bone formation to occur [11–13]. Several strategies have been proposed to develop materials integrated with regenerative growth factors (GFs) [14,15], or GFs delivery systems in order to avoid disruptive side effects [16–20]. One particular example of this technology that saw widespread use is the combination of a simplistic collagen sponge with recombinant human bone morphogenic protein 2 (INFUSE®, Medtronic, Memphis, TN, USA). Unfortunately, off-label use of this product has been fraught with complications ranging from dysphaghia and/or dysphonia to retrograde ejaculation and even a trend toward increased cancer incidence. Perhaps the incidence of adverse effects with the use of such synthetic products could be decreased by improving the biomaterial matrix; or the requisite dose required for effect could be diminished, thus reducing dose-dependent clinical complications [19,21,22].

The ideal material for bone augmentation should not only be osteoconductive but osteoinductive, exploiting the self-healing capabilities of the patient via: (i) recruiting progenitor cells and promoting their proliferation and differentiation; (ii) providing the main structural building blocks for the formation of new tissue; (iii) biocompatibility. The current approach to achieve these goals is biomimicry, which aims to design materials that closely resemble the target tissue [23]. So far, biomimicry has proven a powerful strategy in the development of bone substitutes. The most common examples are based on calcium phosphates (e.g. hydroxyapatite), which is the main component of bone [24,25]. However, bone extracellular matrix (ECM) is also formed by an organic component, which acts as a template for the mineral phase deposition – a process dependent on type I collagen [26]. The structure of the organic matrix has a fundamental role in the mineralization of bone, as it not only directs the mineral deposition, but also guides their growth, by the interaction of its functional groups (e.g. carbonyl groups) [27] with apatite crystals. Such highly regulated chemical-physical interaction between the inorganic and organic phase is fundamental to allow for the formation of a composite material (bone) with unique properties of both stiffness (minerals) and elasticity (collagen) [28]. Also, the hydroxyapatite within bone is characterized by a multitude of doping ions that substitute either calcium or phosphate in the crystal lattice [29]. Magnesium is one of the main ions found in young bone or newly formed bone, which are characterized by a faster turnover [30]. Thus, the simulation of such ECM by synthetic substitutes could theoretically significantly enhance bone formation.

In this study, we aimed to manufacture and characterize a composite material able to recapitulate the chemical-physical and morphological cues of young human osteogenic niche as a potential robust substitute for bone augmentation. Our working hypothesis was that mimicry of the composition and structure of the osteogenic niche within a composite scaffold would facilitate osteogenesis *in vitro* and bone formation at an ectopic site. In an attempt to mimic the newly formed bone niche and test our hypothesis, we developed a bio-inspired, nanocrystalline magnesium-doped hydroxyapatite/type I collagen composite scaffold (MHA/Coll). Its osteoinductive potential was initially determined *in vitro* using human bone marrow-derived mesenchymal stem cells (hBM-MSC) over a 3-week period, then its

effectiveness in promoting new bone formation was assessed *in vivo* using an ectopic rabbit model.

2. Materials and methods

2.1. MHA synthesis

Magnesium-doped hydroxyapatite (MHA) powders were prepared at 37 °C in air atmosphere by dropping 300 mL of an aqueous solution containing 44.4 g of H_3PO_4 (Aldrich, 85% pure) into basic suspensions consisting of 50 g $Ca(OH)_2$ (Aldrich, 95% pure) and different amounts of $MgCl_2 \cdot 6H_2O$ (Merck, A.C.S., ISO) in 500 mL of water. The apatite was let ageing for 24 h at room temperature, then washed with DI water and freeze dried.

2.2. Scaffold synthesis

Type I collagen from bovine tendon (Nitta Casing) was the organic matrix used for the synthesis of MHA/Coll. The collagen was dissolved at a concentration of 10 mg/mL in an aqueous acetic buffer solution at pH 3.5. MHA nanocrystals were directly nucleated on the collagen fibrils, during their pH-driven self-assembling. Briefly, 40 mM aqueous solution of H_3PO_4 was added to 40 g of the acetic collagen gel, and dropped in a aqueous 40 mM basic suspension of $Ca(OH)_2$ and $MgCl_2 \cdot 6H_2O$. $MgCl_2 \cdot 6H_2O$ was added to the basic solution to obtain a teoric 5% sobsitution of calcium in the final apatite lattice the material underwent a wet crosslinking in a aqueous solution of 1,4-butanediol diglycidyl ether (BDDGE) (2.5 mM), at 4 °C. After this step, the material was washed several times with distilled water to eliminate any residual solvent and crosslinking solution. The slurry was adjusted in 48-well plates (2 mm height), to fabricate the scaffold for the *in vitro* studies, while for the *in vivo* studies we utilized a cylindrical mold (4 cm × 1 cm). The final porosity of the scaffold was generated by freeze drying. Briefly, the materials was frozen from +20 °C to −20 °C in 3 h, and then heated from −20 °C to +20 °C in 3 h under vacuum conditions (80 mTorr). Non-mineralized collagen scaffolds (Coll) were also synthesized as described above, from an acetic collagen slurry (10 mg/mL), which was precipitated to pH 5.5 with NaOH (1.67 mM). Collagen was washed with DI as well, and scaffolds were prepared with the same freeze drying process followed for MHA/Coll. All chemicals were purchased from Sigma Aldrich.

2.3. Compositional characterization of MHA/Coll

X-ray diffraction (XRD) patterns were recorded by a Bruker AXS D8 Advance instrument, in reflection mode with Cu Ka radiation. The samples were mounted on a customized support to obtain relatively uniform samples. Fourier-transformed Infrared spectroscopy (FTIR) was performed using a Nicolet 4700 Spectroscopy on pellets (10 mm in diameter) which were prepared by mixing 2 mg of grounded sample with 100 mg of KBr in a mortar and pressing to produce the pellet to be analyzed. Spectra were analyzed by the software EZ OMNIC (Nicolet) after baseline correction.

Inductively coupled plasma – atomic emission spectrometry (ICP-AES: Liberty 200, Varian, Clayton South, Australia), was applied to determine the content of Mg^{2+}, Ca^{2+}, PO_4^{3-} ions constituting the mineral phase forming the composite. Samples were previously prepared by acid attack with nitric acid 65 wt%. The obtained values were expressed in terms of Ca/P and Mg/Ca molar ratios. Thermal gravimetric analysis and differential scanning calorimetry were performed though a TGA/DSC thermogravimetric analyzer (METTLER TOLEDO), by placing the samples in alumina

pans, and undergoing a heating ramp from 25 °C up to 1100 °C, at 10 °C/min.

2.4. Structural characterization of MHA/Coll

Coll and MHA/Coll morphology was evaluated and compared to that of human trabecular bone by scanning electron microscopy (SEM) (Quanta 600 FEG, FEI Company, Hillsboro, OR). Scaffolds were compared to human trabecular bone specimens, which were decellularized and dehydrated according to established protocols [31]. Freeze dried samples were sputter coated with 10 nm of Pt/Pd and imaged at a voltage of 10 mA.

The Atomic Force Microscopy (AFM,Bruker MultiMode 8) measurements were obtained using ScanAsyst-air probes, and the spring constant (Nominal 0.4 N/m, radius 2 nm) and deflection sensitivity has been calibrated. From the bulky scaffold we removed some fibers, we suspend them in MQ water and then we let them dry on a mica surface. All presented AFM images are height and phase data and images within each figure are on the same height scale and have been subject to the 1 order of flattering.

AFM images were collected from different samples and at random spot surface sampling (at least five areas per sample). The quantitative roughness (Ra) data was obtained by Bruker software (NanoScope Analysis) on sampling areas of 100 nm^2, randomly analyzed on 4 different images [32].

Quantitative mechanical characterization was determined using the same instrument, operated under peak-force tapping mode with 1.0 Hz scan rates and a 200 mV amplitude set point. To calculate the Young's modulus, the retract curve of the force versus separation plots could be fitted by the DMT model [33]:

$$F - F_{adh} = 4/3 \ E^* \ \sqrt{R(d - d_0)}^3$$

$F - F_{adh}$ is the force on the cantilever relative to the adhesion force, R is the tip radius, $d - d0$ is the deformation of the sample, and E^* is the reduced modulus. The Young's modulus measurement has been calculated on a sample corresponded to 512×512 force–separation curves obtained over an area $1.7 \ \mu m \times 1.7 \ \mu m$.

2.5. hBM-MSC culture

hBM-MSC cultures were established following the manufacturer's instructions (Gibco). Adherent cells were serially passaged using TripLE™ Express (Invitrogen) upon reaching near confluence (80%) and then reseeded for culture maintenance.

2.6. Cell organization and morphology in 3D culture

To be seeded into scaffolds, hBM-MSC were harvested and resuspended in standard cell culture medium. A drop of 30 μl containing 350,000 cells was seeded on the center of each scaffolds (either collagen or MHA/Coll) and kept in incubator for 10 min. Culture medium was then added to each well. Cell morphology in 2D culture was evaluated by staining with phalloidin and DAPI according to manufacturer's protocols (Life Technology), while in 3D by staining with LIVE/DEAD®. Images were acquired by confocal laser microscopy. The scaffold was imaged exploiting its auto-fluorescence at 358/461 nm. Cell viability on the scaffolds was evaluated by LIVE/DEAD® cell viability assay, which was performed according to manufacturer protocol. Samples were imaged by an Eclipse Ti fluorescence microscope (NIKON) and cell viability was calculated via an automated measurement tool of the NIS-Elements Software (NIKON).

2.7. Cell proliferation on scaffolds

Cell proliferation in the scaffolds was evaluated by Alamar Blue assay (Invitrogen) according to manufacturer's instructions. Absorbance was measured at a wavelength of 570 and 600 nm. Three days after seeding, hBM-MSC were stained using a fluorescent Live-Dead Viability Assay (Molecular Probes, Eugene, OR) according to the manufacturer's instructions and captured on a A1 confocal laser microscope (NIKON).

2.8. hBM-MSC osteogenic differentiation

The osteogenic potential of MHA/Coll has been evaluated over a 21-days period. hBM-MSC at passage 3 were seeded onto Coll and MHA/Coll at the density of 10,000/cm^2. hBM-MSC cultured in 2D conditions, either exposed to inducing media (StemPro® Osteogenesis Differentiation Kit, Gibco) or kept in standard media were used as positive and negative controls, respectively. Media changes were performed every three days.

2.9. Gene expression analysis

To confirm the osteogenic induction, total RNA was isolated from cells grown on scaffolds by homogenization in 1 mL of Trizol reagent (Life Technologies) according to the manufacturer's instructions with a Power Gen 125 tissue homogenizer (Fisher Scientific). For each sample, RNA concentration and purity were measured using Nanodrop Spectrophotometer (Nanodrop® ND1000). Treatment with DNAse (Sigma) was performed to avoid DNA contamination. cDNA was synthesized from 1 μl of total RNA using Taqman Reverse Transcription reagents kit (Applied Biosystems, Branchburg, NJ). Amplifications were set on plates in a final volume of 10 μl and carried out using TaqMan® Fast Advanced Master Mix and TaqMan Probes (Applied Biosystems). The expression of osteocalcin (BGLAP; Hs01587814_g1), osteopontin (SPP1; Hs00959010_m1) and alkaline phosphatase (ALP; Hs01029144_m1) was assessed. The expression of osteogenic specific genes of hBM-MSC cultured on MHA/Coll was compared to that of cells on collagen scaffolds (Coll), and cells cultured in 2D conditions with osteogenic media (MSC-induced), or not (MSC-ctrl). Results were normalized to the level of glyceraldehyde 3-phosphate dehydrogenase (GAPDH; Hs02758991_g1) and represented with respect to MSC-ctrl.

2.10. Subcutaneous implantation of MHA/Coll

Skeletally mature New Zealand white rabbits were used for the purpose of this study. All animals were maintained and used in conformity with the guidelines established by American Association for Laboratory Animal Science (IACUC). In prone position and under the effects of surgical anesthesia; with the use of sterile technique, three incisions were made on the back of each animal. Using blunt dissection, the subcutaneous pockets were created. One scaffold (1 cm diameter x 3 cm long) was implanted subcutaneously into each pocket. Each rabbit was implanted with 3 scaffolds. After placement of implants, the incisions were closed with staples.

2.11. DynaCT analysis of specimens

Under the effects of sedation, lumbosacral computed tomography (DynaCT) scans were obtained from all animals at 24h, 2, 4 and 6 weeks post-surgery. Scanning was performed using a Siemens Axiom Artis C-arm (d)FC (Siemens Healthcare, Erlangen, Germany), with a 48 cm × 36 cm flat-panel integrated detector. Acquisition
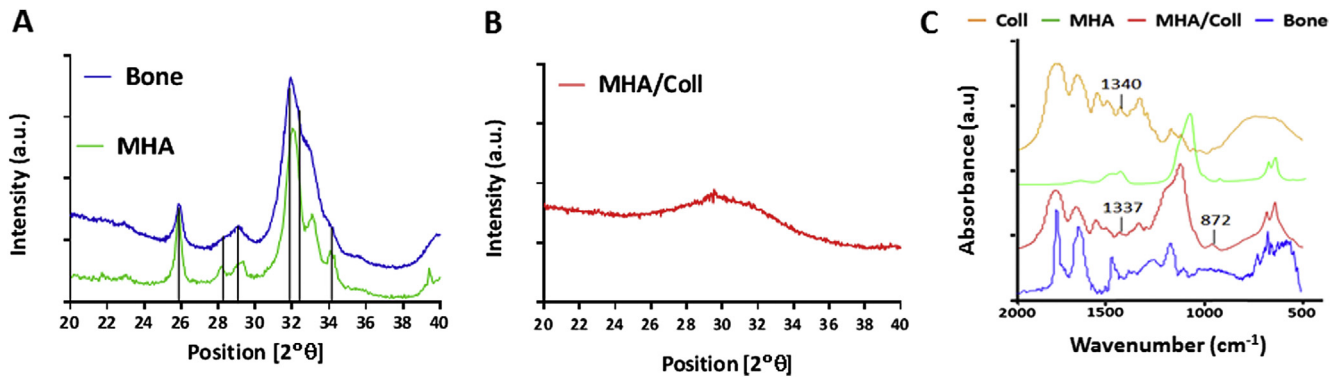
Fig. 1. XRD spectra of human trabecular bone (blue) and MHA (green) (A), compared to MHA/Coll (B). FTIR spectra of Coll, MHA, MHA/Coll respect to that of bone (C). (For interpretation of the references to color in this figure legend, the reader is referred to the web version of this article.)

parameters for DynaCT were as follows: 70 kV tube voltage, automatic tube current of 107 mA, 20 s scan. Each scan entailed 222 degrees of rotation, with 1 image taken every 0.5° for a total of 444 images (each digital acquisition had a matrix of 514x514 pixels) per acquisition. Three-dimensional bone deposition analysis was performed on every CT scan with the use of the Inveon Research Workplace 4.2 Software (Siemen Medical Solution, USA, Inc.).

2.12. Statistical analysis

Statistics were calculated with Prism GraphPad software. Statistics for experiments was performed using a Two-Way ANOVA followed by a Tukey's multiple comparison test. In all cases * was used for $p < 0.05$, ** for $p < 0.01$, and *** for $p < 0.001$, and **** for $p < 0.0001$. All experiments were performed at least in triplicates. Data is presented as mean ± SD.

3. Results

3.1. Characterization of the chemical composition of MHA/Coll

Compared to commercially available stoichiometric hydroxyapatite (Fig. S1), MHA (green) was characterized by low crystallinity, and a similar pattern to that of the mineral phase of human bone (blue), which displayed almost identical shape (Fig. 1A). It was observed, that Bone was slightly more amorphous than bone, as evidenced by broader peaks. However, when such MHA was nucleated, through our biologically inspired mineralization process, onto highly structured type I collagen fibers, the result was the composite MHA/Coll, which displayed a pattern typical of amorphous phases (Fig. 1B).

We further investigated the chemical interaction between the mineral phase MHA and the fibers of collagen with FTIR spectroscopy (Fig. 1C). A shift from 1340 to 1337 cm^{-1} of the band corresponding to the stretching of $-COO^-$ group of collagen was observed, which is representative of collagen's functional group

interacting with the positively charged apatite nanocrystals. The band at 872 cm^{-1}, indicating the carbonation of the MHA that was nucleated on the collagen, resulted more intense.

Table 1 reports the results of the ICP analysis of MHA/Coll. The average value of the Ca/P ratio of MHA nucleated on collagen was 1.561, which is in the range of low crystalline apatite (1.45–1.60); the presence of HPO_4^{2-} in low crystalline apatites is responsible of a decrease in this ratio. The amount of magnesium substituting calcium was about 76% of the starting nominal concentration of magnesium, and resulted in the substitution of 3.78%.

TGA was performed to quantify the amount of mineral phase which could be nucleated on the collagen in the MHA/Coll composite. This experiment revealed that the mineral phase content was the 56 wt% in MHA/Coll, and that it corresponded to that of human trabecular bone (53 wt%) (Fig. 2).

3.2. Morphological characterization of MHA/Coll

Coll and MHA/Coll structures were evaluated by SEM (Fig. 3). Coll scaffold (Fig. 3A) revealed pores in the order of about 200 μm (Fig. 3B), and collagen fibers were highly structured, preserving their typical bands (Fig. 3C). MHA/Coll proved to be very different with respect to Coll at a first gross evaluation (Fig. 3D). Its SEM micrographs showed the presence of more anisotropic pores at lower magnification (Fig. 3E). At higher magnification MHA/Coll appeared significantly different with respect to Coll (Fig. 3F), as pores were not as defined and a more fibrous structure was found. Fig. 3G shows a single fiber of the mineralized collagen of the scaffold MHA/Coll: the collagen fiber appeared wider in diameter, being completely filled and covered by an amorphous mineral
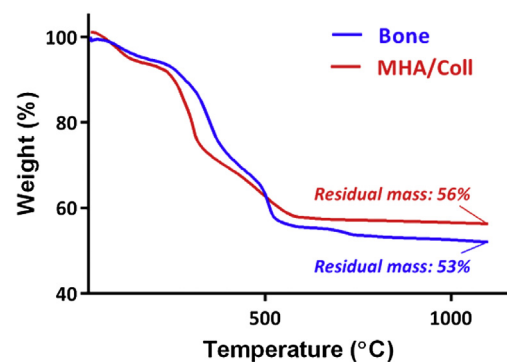
Table 1
Chemical composition of MHA/Coll obtained by ICP-AES.

Sample labels	Ca (A) 422.673	Mg (A) 280.270	PO4 (A) 213.618
Standard 1 ppm	80	5	98
ml	40	2,5	16
MHA/Coll			
ppm	40,429	0,9263	61,398
mole	1009	0.038	0.646
Ca/P	1561		
Ca + Mg/P	1620		
Mg/Ca %	3,78		

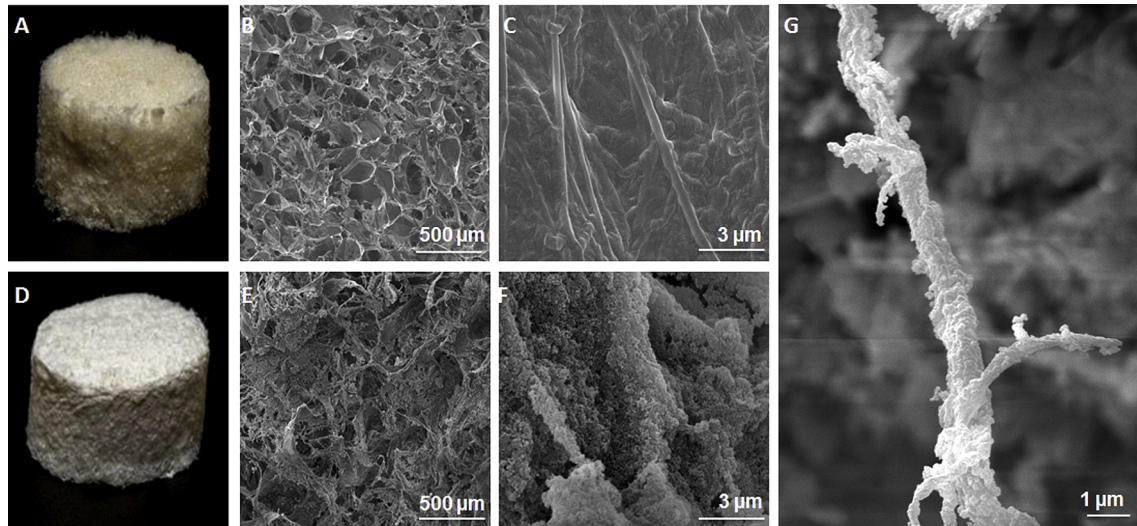**Fig. 2.** Weight percentage of mineral phase nucleated on the collagen in MHA/Coll sample, compared to that of bone, by TGA.

Fig. 3. Picture of Coll (A) and SEM micrographs at 200× (B) and 25000× (C). Photography of MHA/Coll (D) and SEM micrographs at the two different magnifications, respectively (E, F). SEM image of a collagen fiber of MHA/Coll, completely mineralized (G).

phase, and not simply mixed with hydroxyapatite particles (Fig. S2). MHA/Coll morphology and structure appeared significantly similar to that of decellularized human trabecular bone, which displayed comparable fibrous structure and roughness (Fig. 4).

3.3. Nano-structural and nano-mechanical characterization of MHA/Coll

Fig. 5 resembles the measurements acquired by AFM. Fig. 5A and B shows Coll and MHA/Coll small bundle of fibers in 2 and 3D representation. Coll appeared as a compacted and regular grouped fibers characterized by the typical collagen banding (see arrows in Fig. 5A) of ~62 nm pattern. MHA/Coll presented a more structured surface in which the banding has been covered by the MHA crystals. However, a recurrent pattern has been found also MHA/Coll with a periodicity of ~89 nm. Mean roughness (Ra) of Coll was 18.5 ± 0.8 nm which rose four times in the case of MHA/Coll (65.95 ± 0.21 nm) as reported in the graph in Fig. 5C. We used a surface mapping technique called PeakForce QNM AFM in order to evaluate the nanomechanical features of the fibers of the two different materials as previously reported [33]. Figs. 5D and E, the representative sample from Coll and MHA/Coll possessed a similar modulus distribution, ~2 GPa. However, Coll showed a less homogenous modulus in comparison with MHA/Coll as evidenced by the higher standard deviation (Fig. 5F).

3.4. hBM-MSC morphology and viability on MHA/Coll

The morphology of hBM-MSC cultured in 2D conditions (Fig. 6A) was significantly different than that of cells grown on 3D collagen scaffolds, in which there was apparent alignment along the fibers (Fig. 6B), in an "Indian file" conformation (see also magnification, Fig. 6C). Cell viability on Coll and MHA/Coll was assessed by LIVE/DEAD® assay. Cell distribution and organization on the scaffolds was found to be different between Coll and MHA/Coll. Cells appeared to align along the pores' wall of both Coll and MHA/Coll at 24h (Figs. 6C and D, respectively). Cells on Coll and MHA/Coll remained alive for up to 7 days (Fig. 6E and F respectively), with viability >90% (Fig. 6G).

Cell growth was also assessed at 1 week and compared to hBM-MSC cultured in 2D conditions (CTRL), as positive control. While CTRL cells grew at a constant rate over the 7 days, MHA/Coll showed the lowest rate of cell growth with respect to CTRL and Coll (less than 40% reduction at 1 week) (Fig. 6H).

3.5. Osteogenic induction in vitro

We cultured hBM-MSCs onto MHA/Coll scaffolds in order to evaluate the expression of osteogenesis-associated genes (Fig. 7). The expression levels increased to 78.62 (±4.54)-fold for *Bglap*, 17.87 (±1.35)-fold for *Alp*, and 46.12 (±4.55)-fold for *Spp1* compared to the uninduced 2D counterparts (MSC-ctrl) and were found even
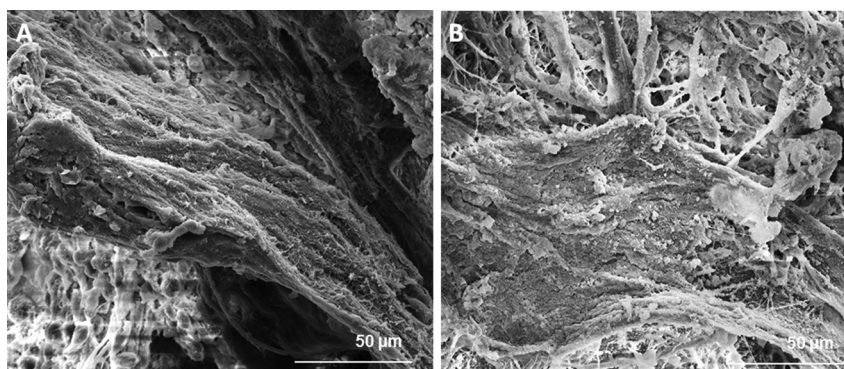

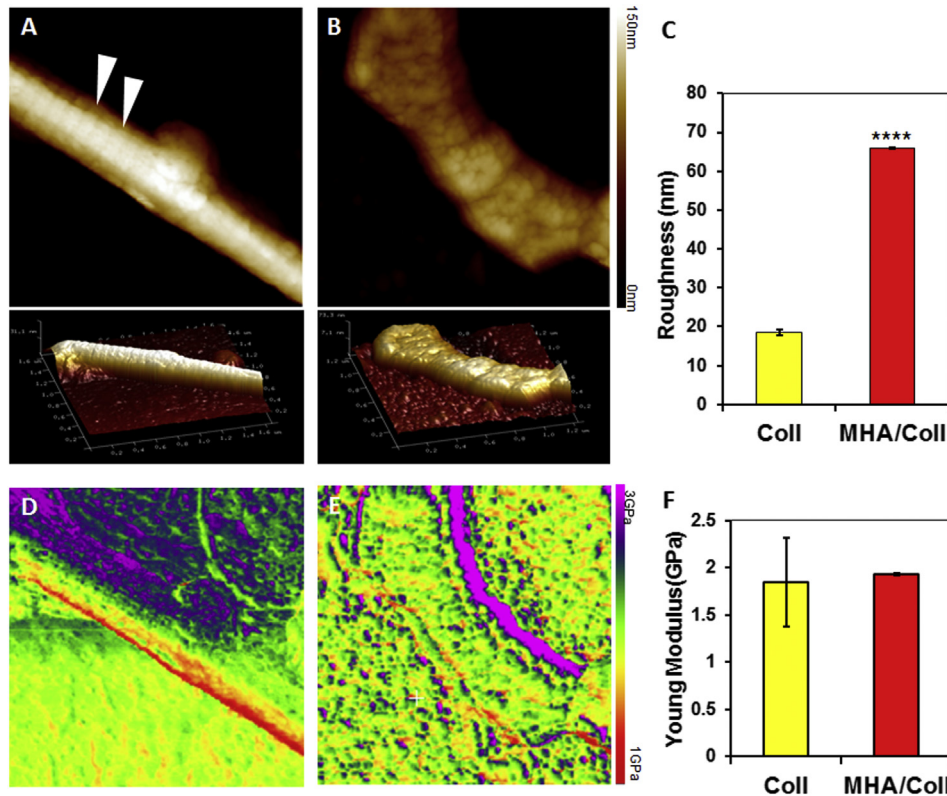**Fig. 4.** SEM micrographs of human trabecular bone (A) and MHA/Coll (B).

Fig. 5. A–B) 2 and 3D representation of Coll and MHA/Coll images at AFM. The biomineralization of collagen resulted in homogenous mineralized nanofibers assembled of paralleled submicrofibrils. MHA/Coll showed a recurrent pattern of 89 ± 1.2 nm similar to the gap zones of bare collagen (62 ± 2.2 nm). C–D) Property map of Young's modulus of a representative sample. Between the arrows is a single collagen nanofiber with a low modulus. Asterisk: mica base. B) Property map of Young's modulus of a representative EFM sample. Cross-banding could be identified in some fibrils with a different distribution of moduli (open arrowhead versus arrows). C) Property map of Young's modulus of a representative sample, showing the uniform distribution of the modulus for MHA/Coll. D) Graph represent the Roughness (Ra) Young's modulus of Coll (yellow) and MHA/Coll (red). (For interpretation of the references to color in this figure legend, the reader is referred to the web version of this article.)

higher than those observed when cells were exposed to inducing media (MSC-induced). The expression levels in hBM-MSC grown onto collagen scaffolds (Coll) were comparable to those observed in uninduced hBM-MSC expanded in 2D conditions.

3.6. Ectopic bone formation

There were no surgical complications secondary to the operations performed and all experimental animals tolerated the procedure quite well. Over the course of the 6-week postoperative period, a palpable change in density and firmness in the implanted scaffolds could be easily appreciated on gross clinical exam, confirmed by neutral parties (veterinary technicians within the HMRI Comparative Medicine Department). As expected, due to the high porosity of MHA/Coll, with a density slightly higher than that of air, extracorporeal scaffolds displayed no quantifiable volume at the requisite density thresholds. However, at 24 h post-implantation, the average volume at 200 HU threshold was 69 mm^3 (±9.8), which was used as baseline and all subsequent measurements had this value subtracted from the total. As expected, the volume at 500 HU threshold at 24 h was zero. It was found that MHA/Coll enabled for the production of a large extent of spongy bone tissue, with a volume of approximately 2 cm^3, in just 4 weeks. In details, over the course of the 6-week study period, the scaffolds demonstrated increasing volumes of bone formation, with a bell curve distribution of trabecular (200 HU) bone peaking at 4 weeks (818.4 mm^3 ± 130.9), before decreasing at 6 weeks to 597.54 mm^3 (±176.8) (Fig. 8). Interestingly, this temporal change in trabecular bone volume inversely mirrors the trend for cortical-

type bone (500 HU) throughout the study, which gradually increased from nearly nothing at 2 weeks (0.80 mm^3) to 75.3 mm^3 at the final time point (Fig. S4).

4. Discussion

The present work investigated the osteoinductive potential of a scaffold mimicking the osteogenic niche of human trabecular bone, for bone augmentation. MHA/Coll was synthesized through an innovative biologically inspired process, resembling the main steps of biomineralization [34]. During material's fabrication, the osteogenic niche of newly formed bone is mimicked, by partially substituting calcium with magnesium in the apatite lattice. Besides being poorly crystalline, biological apatite presents substitutions in the hydroxyapatite lattice structure, and presents doping cations and anions. Magnesium is the most abundant ion in bone, typically present in an extent of 5% during osteogenesis (e.g. newly formed bone, young bone), while it tends to disappear in mature and aging bone [28]. Therefore, by introducing this ion in apatite's structure, it is possible to reproduce the conditions found during osteogenesis.

Firstly, the overall morphology of the scaffold, mineral phase composition and extent were compared to those of human bone. Secondly, the scaffold's ability to trigger specific cell functions, such as cell organization and the expression of osteoblastogenesis-associated genes in hBM-MSC was studied. Finally, after assessing its potential to recapitulate the osteogenic niche *in vitro*, we investigated the capability of MHA/Coll scaffolds to induce bone formation in an ectopic model in rabbit.

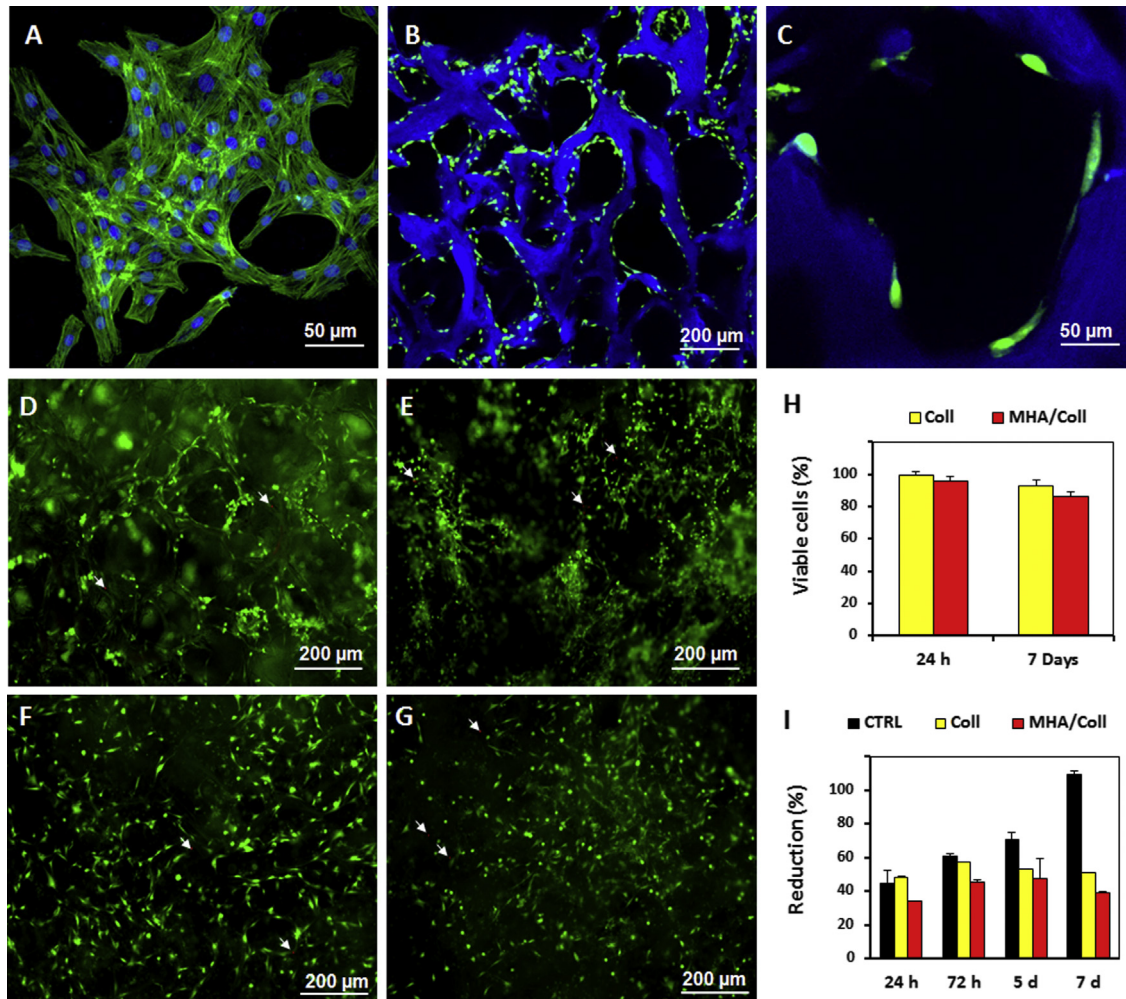The process of natural biomineralization in bone is finely

Fig. 6. Confocal laser micrographs of hBM-MSC seeded in 2D cultures (A), compared with cells cultured in 3D conditions on collagen-based scaffolds (B); magnification of cell morphology and organization in 3D culture (C). Fluorescence microscopy images of cells stained with LIVE/DEAD®, seeded on Coll (D, E) and MHA/Coll (F, G) at 24 h and 7 days respectively. The white arrows indicate few dead cells. Quantification of viable cells (H) and cell growth on the scaffolds (I).
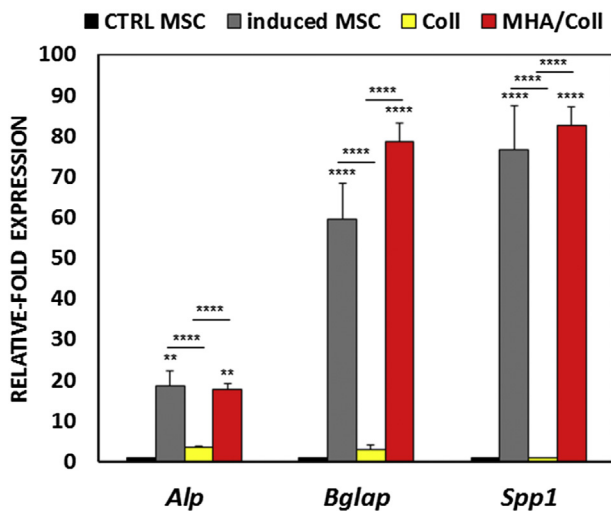

Fig. 7. qPCR analysis for the expression of the osteogenic (Alp, Bglap, Ssp1) markers for hBM-MSC grown in 2D conditions (MSC and induced MSC) and onto scaffolds (Coll and MHA/Coll). Data are represented as fold-change compared with the expression levels found in the uninduced MSC. Values are mean ± SD (n = 3). Asterisks depict highly significant differences (P < 0.01).

controlled via chemical, physical, morphological and structural mechanisms [35]. The chemical control consists of the precipitation of ions, naturally present in the bone niche (e.g. Ca^{2+}, CO_3^{2-}, Na^+, K^+), on the organic ECM (mainly collagen), contributing to hydroxyapatite crystals' morphology and orientation [36]. The presence and spatial distribution of functional groups on the template's surface allows for the structural control over crystals' preferential growth along collagen fibers, and finally, a morphologic control results from the previous control mechanisms, by ensuring a specific architecture of the mineral phase up to the macroscale level. These multiscale control mechanisms ensure the proper homeostasis of bone, at the chemical, physical, morphological and structural level [34,37]. In this study, scaffold's fabrication differed from the most common preparation of composite materials, as type I collagen was dispersed in acetic solution and dropped in the basic solution of $Ca(OH)_2$ and $MgCl_2 \cdot 6H_2O$. Under these controlled conditions of pH, collagen fibers assembled during the precipitation of the calcium phosphate phase [34]. This resulted in a composite material which more closely resembled human trabecular bone's morphology (Fig. 4). We demonstrated by a direct comparison with human trabecular bone that this MHA/Coll mimics for composition and overall structure of bone.

The chemical composition of human trabecular bone was also proven to be closely mimicked by MHA/Coll, by characterization
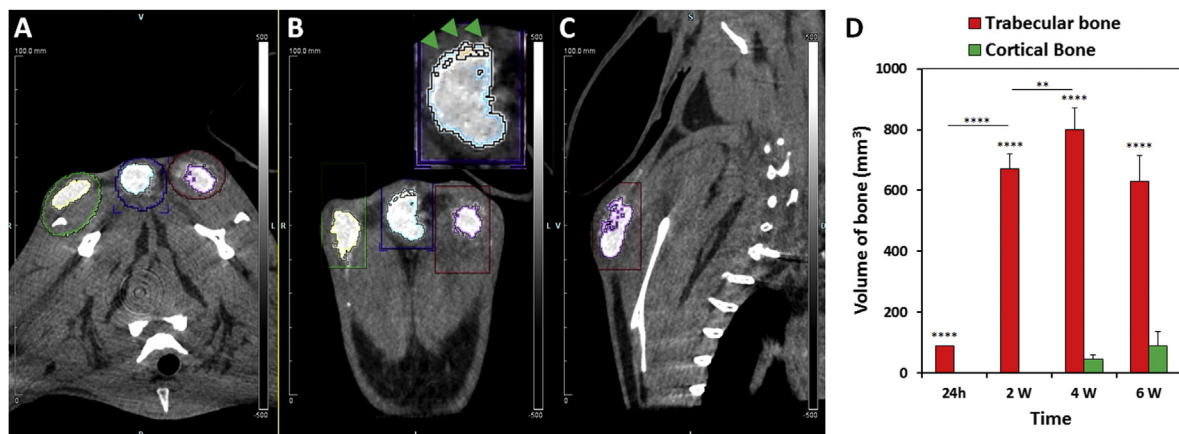
Fig. 8. DynaCT scan of MHA/Coll seeded subcutaneously in rabbit, at 4 weeks, (A, B, C). Inset in figure B showed area of cortical bone in the edges of the scaffold, indicated by green arrows. Bone mass volume formed in the ectopic site in rabbit at 24h, 2, 4 and 6 weeks (D). (For interpretation of the references to colour in this figure legend, the reader is referred to the web version of this article.)

with XRD. Both spectra presented the typical peaks of hydroxyapatite (indicated), and also coincided (Fig. 1A). Our biomimetic apatite phase presented the same composition and level of crystallinity of that of human bone. MHA spectra were also acquired after nucleation on highly structured type I collagen through our bio-inspired process. It resulted in crystallinity significantly decreasing when in the composite MHA/Coll. Collagen, acting as a template for the nucleation of the crystals of apatite, as in the natural biomineralization process, prevented their growth, inducing the formation of nanostructured hydroxyapatite. Low crystallinity is due not only to the presence of nano-sized crystals, but also to the incorporation of doping ions (e.g. Mg^{2+}, CO_3^{2-}, HPO_4^{2-}) in apatite's lattice, as it occurs in the bone niche, where a multiplicity of ions are present [30]. Doping ions' role in maintain the low crystallinity of bone apatite is crucial for bone metabolism [37]. In fact, the decrease in crystallinity was reported to correspond to higher reactivity in vivo, which determines faster bone formation and remodeling [38]. The creation of a true MHA/Coll composite, and of a multisubstituted-apatite phase was confirmed by FTIR spectroscopy in which we observed a shift of the peak corresponding to the stretching of $-COO^-$ group of collagen, from 1340 to 1334 cm^{-1}. This switching indicated the binding of MHA with amid I and/or COO- and form $(C=O)_2Ca$ and/or $(COO)_2Ca$ bonds. Also, in MHA/Coll the three characteristic groups of peaks typical of the carbonation in B position of hydroxyapatite were spotted (1540, 1455, 1413 and 879-872 cm^{-1}) [39]. A similar pattern of peaks was observed for both MHA/Coll and bone, further proving the high level of biomimicry of MHA/Coll to the natural tissue (Fig. S3).

Magnesium substitution of calcium was finally confirmed by the Ca/P ratio obtained by ICP analysis, typical of calcium deficient apatite (1.5–1.67) [40]. Magnesium was found to be approximately the 4 mol%, which is significantly similar to that of newly formed bone. Finally, the overall mineral content in MHA/Coll composite was found to coincide with that of decellularized human trabecular bone at approximately 56 wt% (Fig. 5).

Through the biologically inspired mineralization process utilized in this study, we were able to fabricate a composite scaffold which appeared highly porous, with pores of approximately 100–250 μm in diameter, and an overall anisotropic porosity. Furthermore, at the microscale level it was difficult to discriminate between MHA/Coll and human bone trabecular, as they appeared extremely similar (Fig. 4).

AFM confirmed important structural features of MHA/Coll. From the analysis of fibers nanostructure the crystals of MHA are homogeneously nucleated along all the fibers, resulting in a higher Ra induced by the presence of nanocrystals all around collagen surface. In addition the pattern (~89 nm) found in MHA/Coll is probably due to the fact that MHA substitute water in the gap zones used the collagen as organic matrix to start the mineral phase nucleation as well as a natural process of biomineralization [34]. Moreover the presence of the mineral phase affects the nano-mechanical features of the materials. Although the modulus did not show significant difference between the two samples, a more homogenous modulus is showed on MHA/Coll fibers. The mechanical properties of a self-assembled structure strictly depends on the hierarchical organization of the single compounds [41]. The process of synthetic biomineralization provided a higher level of hierarchical organization resulting in homogenous nanomechanical features.

Bone is a dynamic organ where osteoprogenitor cells reorganize and receive a number of structural, physical and paracrine factors able to induce osteoblast, osteocyte or osteoclast differentiation [42,43]. After verifying the resemblance of our material to human trabecular bone, we assessed the ability of our material to retain the functional properties of bone niche and trigger cell specification toward the osteogenic lineage. Despite the cortical [44,45] and trabecular [46–48] portions of the bone having been recently suggested as the major reserve of more potent osteoprogenitor cells, we chose to test this hypothesis using hBM-MSC, due to well-established isolation and expansion protocols [49–51], and the fact that they have been extensively designated as the gold standard in both preclinical and clinical settings [52].

Cells promptly adhered onto the material, which proved to be biocompatible, and were found completely reorganized few days after being seeded. On MHA/Coll, however, cell growth was found lower than Coll. This reinforces the role of our material in recapitulating the osteoblastic niche. In fact, the hypoxic conditions found in the bone have been proposed to be responsible for maintaining the cells in a quiescent state [44], and quiescence of progenitor cells within the niche has been directly linked to their ability to induce an efficient tissue reconstitution [53]. Consistent with this, a significant increase in the expression of osteoblastogenesis-associated markers (Spp1 and Bglap) was found compared with the levels observed in Coll. Interestingly, MHA/Coll resulted in even higher osteocalcin and osteopontin expression than the group represented by induced cells following established in vitro protocols (for p < 0.01).

Finally, we wanted to verify if this higher level of biomimicry could allow for more efficient bone formation *in vivo*, in a large animal model (rabbit). MHA/Coll's osteoinductive potential to form an extended bone mass more efficiently, without the addition of any bioactive molecule or cells, was evaluated in an ectopic model. There is a crucial difference between bone formation in an orthotopic and ectopic model. In an orthotopic site, bone regeneration mediated by a scaffold it is strongly facilitated. In fact, after the creation of the surgical defect and scaffold implantation, follows the activation of endogenous cascades of signaling pathways that induce the in situ release of osteogenic GFs [54—56]. The upregulation of these pathways have been demonstrated to be crucial for bone repair mediated by MSC [57]. Furthermore, in orthotopic models the scaffolds are exposed to mechanical forces [58], which has been reported to positively affect the final outcome [59]. On the other hand, there is much evidence that using cellularized scaffold with BM-MSC, bone formation has been achieved around 8 weeks [60—62]. More recently, Kinard and coworkers proposed a synthetic biodegradable hydrogel for the delivery of demineralized bone matrix, to repair a calvarial bone defect in rat (8 mm × 1 mm). They obtained the maximum bone mass formation at 12 weeks [63].

On the contrary, in ectopic models most osteogenic stimuli, such as cytokines, bone cells, autologous stem cells and mechanotransduction are eliminated (or significantly reduced) [56].

Recently, other significant articles about bone augmentation in rabbit have been published. Kim and coworkers reported the regeneration of a critical sized calvarial defect in rabbit, in 6 weeks, by using a polycarbonate scaffold [57]. In this study, we tested our scaffold in an ectopic model, in order to evaluate its intrinsic osteoinductive abilities, eliminating the contribution of endogenous osteogenic stimuli in rabbit that showed a similar mineral density to the human bone in comparison to other rodents models [64].

The most striking *in vivo* result was the dramatic mass (approximately 2 cm × 1 cm x 1 cm) of bone formed in only 2 weeks, which is a third or even a sixth (depending on the material and animal model) of the time usually necessary for scaffolds to produce bone-like tissue. Remarkably, these results were achieved without the contribution of endogenous cytokines (since the scaffold was implanted subcutaneously), heterologous cytokines, or addition of progenitor cells on the scaffold. Furthermore, the maturation of this bone mass initiated at only 6 weeks.

To our knowledge, this study reports for the first time the formation of extend mass of trabecular bone in an ectopic model in large animal by an innovative composite scaffold. This study represents a significant accomplishment for the field of bone augmentation, as no robust off-the-shelf approach is currently available.

5. Conclusions

In this study MHA/Coll composite scaffold was synthesized through an innovative biologically inspired process, resembling the main steps of the biomineralization. It was investigated if such synthetic material could mimic the osteogenic niche at the chemical, physical, morphological and biological level, and its potential was ultimately assessed in a large animal model.

Altogether, data reported in this study represents a significant step in the development of acellular off-the-shelf substitutes for applications of bone augmentation. By simply mimicking the osteogenic niche from the nanoscale up to the macroscale of the bone ECM, this scaffold was shown to actively induce stem cells osteogenic specification *in vitro*, while providing an osteoconductive environment for tissue remodeling. This approach would significantly impact the orthopedic field, as it represents a robust alternative to the currently available materials, and to the use of osteoinductive molecules, such as human recombinant BMP-2 whose use is still highly controversial.

Appendix A. Supplementary data

Supplementary data related to this article can be found at http://dx.doi.org/10.1016/j.biomaterials.2015.05.011.

References

[1] B.S. McAllister, K. Haghighat, Bone augmentation techniques, J. Periodontol. 78 (2007) 377—396.

[2] M. Chiapasco, P. Casentini, M. Zaniboni, Bone augmentation procedures in implant dentistry, Int. J. oral Maxillofac. implants 24 (2008) 237—259.

[3] D.J. Hak, The use of osteoconductive bone graft substitutes in orthopaedic trauma, J. Am. Acad. Orthop. Surg. 15 (2007) 525—536.

[4] E.D. Arrington, W.J. Smith, H.G. Chambers, A.L. Bucknell, N.A. Davino, Complications of iliac crest bone graft harvesting, Clin. Orthop. Relat. Res. 329 (1996) 300—309.

[5] R.W. Bucholz, Nonallograft osteoconductive bone graft substitutes, Clin. Orthop. Relat. Res. 395 (2002) 44—52.

[6] J.S. Silber, D.G. Anderson, S.D. Daffner, B.T. Brislin, J.M. Leland, A.S. Hilibrand, et al., Donor site morbidity after anterior iliac crest bone harvest for single-level anterior cervical discectomy and fusion, Spine 28 (2003) 134—139.

[7] P.V. Giannoudis, H. Dinopoulos, E. Tsiridis, Bone substitutes: an update, Injury 36 (2005) S20—S27.

[8] G. Zimmermann, A. Moghaddam, Allograft bone matrix versus synthetic bone graft substitutes, Injury 42 (2011) S16—S21.

[9] Y. Khan, M.J. Yaszemski, A.G. Mikos, C.T. Laurencin, Tissue engineering of bone: material and matrix considerations, J. Bone Jt. Surg. 90 (2008) 36—42.

[10] A.S. Greenwald, S.D. Boden, V.M. Goldberg, Y. Khan, C.T. Laurencin, R.N. Rosier, Bone-graft substitutes: facts, fictions, and applications, J. Bone Jt. Surg. 83 (2001) S98—S103.

[11] L.S. Nair, C.T. Laurencin, Biodegradable polymers as biomaterials, Prog. Polym. Sci. 32 (2007) 762—798.

[12] M. Kellomäki, H. Niiranen, K. Puumanen, N. Ashammakhi, T. Waris, P. Törmälä, Bioabsorbable scaffolds for guided bone regeneration and generation, Biomaterials 21 (2000) 2495—2505.

[13] D.W. Hutmacher, Scaffolds in tissue engineering bone and cartilage, Biomaterials 21 (2000) 2529—2543.

[14] D.H. Kempen, L. Lu, A. Heijink, T.E. Hefferan, L.B. Creemers, A. Maran, et al., Effect of local sequential VEGF and BMP-2 delivery on ectopic and orthotopic bone regeneration, Biomaterials 30 (2009) 2816—2825.

[15] P. Yilgor, K. Tuzlakoglu, R.L. Reis, N. Hasirci, V. Hasirci, Incorporation of a sequential BMP-2/BMP-7 delivery system into chitosan-based scaffolds for bone tissue engineering, Biomaterials 30 (2009) 3551—3559.

[16] M. Manassero, V. Viateau, M. Deschepper, K. Oudina, D. Logeart-Avramoglou, H. Petite, et al., Bone regeneration in sheep using acropora coral, a natural resorbable scaffold, and autologous mesenchymal stem cells, Tissue Eng. Part A 19 (2013) 1554—1563.

[17] S. Bose, M. Roy, A. Bandyopadhyay, Recent advances in bone tissue engineering scaffolds, Trends Biotechnol. 30 (2012) 546—554.

[18] M. Biondi, F. Ungaro, F. Quaglia, P.A. Netti, Controlled drug delivery in tissue engineering, Adv. Drug Deliv. Rev. 60 (2008) 229—242.

[19] E.J. Carragee, E.L. Hurwitz, B.K. Weiner, A critical review of recombinant human bone morphogenetic protein-2 trials in spinal surgery: emerging safety concerns and lessons learned, Spine J. 11 (2011) 471—491.

[20] S. Minardi, M. Sandri, J.O. Martinez, I.K. Yazdi, X. Liu, M. Ferrari, et al., Multiscale patterning of a biomimetic scaffold integrated with composite microspheres, Small 10 (19) (2014) 3943—3953.

[21] N.E. Epstein, Complications due to the use of BMP/INFUSE in spine surgery: the evidence continues to mount, Surg. Neurol. Int. 4 (2013) S343.

[22] R. Fu, S. Selph, M. McDonagh, K. Peterson, A. Tiwari, R. Chou, et al., Effectiveness and harms of recombinant human bone morphogenetic protein-2 in spine fusion: a systematic review and meta-analysis, Ann. Intern. Med. 158 (2013) 890–902.

[23] J. Patterson, M.M. Martino, J.A. Hubbell, Biomimetic materials in tissue engineering, Mater. Today 13 (2010) 14–22.

[24] S. Bose, S. Tarafder, Calcium phosphate ceramic systems in growth factor and drug delivery for bone tissue engineering: a review, Acta Biomater. 8 (2012) 1401–1421.

[25] A.J. Wagoner Johnson, B.A. Herschler, A review of the mechanical behavior of CaP and CaP/polymer composites for applications in bone replacement and repair, Acta Biomater. 7 (2011) 16–30.

[26] L.G. Raisz, Physiology and pathophysiology of bone remodeling, Clin. Chem. 45 (1999) 1353–1358.

[27] E.P. Katz, S.-T. Li, Structure and function of bone collagen fibrils, J. Mol. Biol. 80 (1973) 1–15.

[28] J. De Bruijn, C. Klein, K. De Groot, C. Van Blitterswijk, The ultrastructure of the bone-hydroxyapatite interface in vitro, J. Biomed. Mater. Res. 26 (1992) 1365–1382.

[29] L. Bertinetti, C. Drouet, C. Combes, C. Rey, A. Tampieri, S. Coluccia, et al., Surface characteristics of nanocrystalline apatites: effect of Mg surface enrichment on morphology, surface hydration species, and cationic environments, Langmuir 25 (2009) 5647–5654.

[30] E. Landi, G. Logroscino, L. Proietti, A. Tampieri, M. Sandri, S. Sprio, Biomimetic Mg-substituted hydroxyapatite: from synthesis to in vivo behaviour, J. Mater. Sci. Mater. Med. 19 (2008) 239–247.

[31] E. Kheir, T. Stapleton, D. Shaw, Z. Jin, J. Fisher, E. Ingham, Development and characterization of an acellular porcine cartilage bone matrix for use in tissue engineering, J. Biomed. Mater. Res. Part A 99 (2011) 283–294.

[32] F. Taraballi, S. Wang, J. Li, F.Y.Y. Lee, S.S. Venkatraman, W.R. Birch, et al., Understanding the nano-topography changes and cellular influences resulting from the surface adsorption of human hair keratins, Adv. Healthc. Mater. 1 (2012) 513–519.

[33] Y. Liu, D. Luo, X.-X. Kou, X.-D. Wang, F.R. Tay, Y.-L. Sha, et al., Hierarchical intrafibrillar nanocarbonated apatite assembly improves the nanomechanics and cytocompatibility of mineralized collagen, Adv. Funct. Mater. 23 (2013) 1404–1411.

[34] A. Tampieri, S. Sprio, M. Sandri, F. Valentini, Mimicking natural biomineralization processes: a new tool for osteochondral scaffold development, Trends Biotechnol. 29 (2011) 526–535.

[35] S. Mann, Biomineralization, Oxford University Press, Oxford, 2001.

[36] F. Nudelman, K. Pieterse, A. George, P.H. Bomans, H. Friedrich, L.J. Brylka, et al., The role of collagen in bone apatite formation in the presence of hydroxyapatite nucleation inhibitors, Nat. Mater. 9 (2010) 1004–1009.

[37] S.S.M. Sprio, S. Panseri, M. Iafisco, A. Ruffini, S. Minardi, A. Tampieri, Bone substitutes based on biomineralization, in: Bone Substitutes Biomaterials, Woodhead Publishing, 2014.

[38] S. Sprio, A. Tampieri, E. Landi, M. Sandri, S. Martorana, G. Celotti, et al., Physico-chemical properties and solubility behaviour of multi-substituted hydroxyapatite powders containing silicon, Mater. Sci. Eng. C 28 (2008) 179–187.

[39] E. Landi, G. Celotti, G. Logroscino, A. Tampieri, Carbonated hydroxyapatite as bone substitute, J. Eur. Ceram. Soc. 23 (2003) 2931–2937.

[40] S.-C. Liou, S.-Y. Chen, H.-Y. Lee, J.-S. Bow, Structural characterization of nano-sized calcium deficient apatite powders, Biomaterials 25 (2004) 189–196.

[41] F. Gelain, D. Silva, A. Caprini, F. Taraballi, A. Natalello, O. Villa, et al., BMHP1-derived self-assembling peptides: hierarchically assembled structures with self-healing propensity and potential for tissue engineering applications, ACS Nano 5 (2011) 1845–1859.

[42] R. Hattner, B.N. Epker, H.M. Frost, Suggested sequential mode of control of changes in cell behaviour in adult bone remodelling, Nature 206 (1965) 489–490.

[43] H. Takayanagi, Osteoimmunology: shared mechanisms and crosstalk between the immune and bone systems, Nat. Rev. Immunol. 7 (2007) 292–304.

[44] B. Corradetti, F. Taraballi, S. Powell, D. Sung, S. Minardi, M. Ferrari, et al., Osteoprogenitor cells from bone marrow and cortical bone: understanding how the environment affects their fate, Stem Cells Dev. 24 (9) (2014) 1112–1123.

[45] H. Zhu, Z.K. Guo, X.X. Jiang, H. Li, X.Y. Wang, H.Y. Yao, et al., A protocol for isolation and culture of mesenchymal stem cells from mouse compact bone, Nat. Protoc. 5 (2010) 550–560.

[46] Y. Sakaguchi, I. Sekiya, K. Yagishita, S. Ichinose, K. Shinomiya, T. Muneta, Suspended cells from trabecular bone by collagenase digestion become virtually identical to mesenchymal stem cells obtained from marrow aspirates, Blood 104 (2004) 2728–2735.

[47] V. Sottile, C. Halleux, F. Bassilana, H. Keller, K. Seuwen, Stem cell characteristics of human trabecular bone-derived cells, Bone 30 (2002) 699–704.

[48] R. Tuli, S. Tuli, S. Nandi, M.L. Wang, P.G. Alexander, H. Haleem-Smith, et al., Characterization of multipotential mesenchymal progenitor cells derived from human trabecular bone, Stem Cells 21 (2003) 681–693.

[49] M. Honczarenko, Y. Le, M. Swierkowski, I. Ghiran, A.M. Glodek, L.E. Silberstein, Human bone marrow stromal cells express a distinct set of biologically functional chemokine receptors, Stem Cells 24 (2006) 1030–1041.

[50] M. Krampera, L. Cosmi, R. Angeli, A. Pasini, F. Liotta, A. Andreini, et al., Role for interferon-gamma in the immunomodulatory activity of human bone marrow mesenchymal stem cells, Stem Cells 24 (2006) 386–398.

[51] M.F. Pittenger, A.M. Mackay, S.C. Beck, R.K. Jaiswal, R. Douglas, J.D. Mosca, et al., Multilineage potential of adult human mesenchymal stem cells, Science 284 (1999) 143–147.

[52] A.J. Friedenstein, J.F. Gorskaja, N.N. Kulagina, Fibroblast precursors in normal and irradiated mouse hematopoietic organs, Exp. Hematol. 4 (1976) 267–274.

[53] T. Yin, L. Li, The stem cell niches in bone, J. Clin. Invest 116 (2006) 1195–1201.

[54] G.J. Schmid, C. Kobayashi, L.J. Sandell, D.M. Ornitz, Fibroblast growth factor expression during skeletal fracture healing in mice, Dev. Dyn. 238 (2009) 766–774.

[55] K. Sarahrudi, A. Thomas, M. Mousavi, G. Kaiser, J. Köttstorfer, M. Kecht, et al., Elevated transforming growth factor-beta 1 (TGF-β1) levels in human fracture healing, Injury 42 (2011) 833–837.

[56] M.A. Scott, B. Levi, A. Askarinam, A. Nguyen, T. Rackohn, K. Ting, et al., Brief review of models of ectopic bone formation, Stem Cells Dev. 21 (2011) 655–667.

[57] B. Levi, A.W. James, E.R. Nelson, M. Peng, D.C. Wan, G.W. Commons, et al., Acute skeletal injury is necessary for human adipose-derived stromal cell mediated calvarial regeneration, Plastic Reconstr. Surg. 127 (2011) 1118.

[58] S. Kuroda, R. Wazen, P. Moffatt, E. Tanaka, A. Nanci, Mechanical stress induces bone formation in the maxillary sinus in a short-term mouse model, Clin. oral Investig. 17 (2013) 131–137.

[59] A.C. Allori, A.M. Sailon, J.H. Pan, S.M. Warren, Biological basis of bone formation, remodeling, and repair-part III: biomechanical forces, Tissue Eng. Part B: Rev. 14 (2008) 285–293.

[60] H. Bahar, A. Yaffe, A. Boskey, I. Binderman, Influence of bone-derived matrices on generation of bone in an ectopic rat model, J. Orthop. Res. 28 (2010) 664–670.

[61] D. Ma, H. Yao, W. Tian, F. Chen, Y. Liu, T. Mao, et al., Enhancing bone formation by transplantation of a scaffold-free tissue-engineered periosteum in a rabbit model, Clin. Oral Implants Res. 22 (2011) 1193–1199.

[62] A. Matsushima, N. Kotobuki, M. Tadokoro, K. Kawate, H. Yajima, Y. Takakura, et al., Vivo osteogenic capability of human mesenchymal cells cultured on hydroxyapatite and on β-tricalcium phosphate, Artif. Organs 33 (2009) 474–481.

[63] L.A. Kinard, R.L. Dahlin, J. Lam, S. Lu, E.J. Lee, F.K. Kasper, et al., Synthetic biodegradable hydrogel delivery of demineralized bone matrix for bone augmentation in a rat model, Acta Biomater. 10 (2014) 4574–4582.

[64] A. Pearce, R. Richards, S. Milz, E. Schneider, S. Pearce, Animal models for implant biomaterial research in bone: a review, Eur. Cell. Mater. 13 (2007) 1–10.